INVESTIGATION AND PREDICTION OF SURFACE INTEGRITY INDUCED BY MILLING OF HOT FORGED AND HEAT TREATED AA7075

Gorkem Tok[a], Ammar Tarık Dincer[b], Ali Taner Kuzu[c] , Mustafa Bakkal[d],

[a] *Istanbul Technical University, Mechanical Engineering Faculty, 34437, Istanbul, Turkey, tokg15@itu.edu.tr*
[b] *Istanbul Technical University, Mechanical Engineering Faculty, 34437, Istanbul, Turkey, ammar.dincer@itu.edu.tr*
[c] *Isik University, Department of Mechanical Engineering, Istanbul, Turkey, alitaner.kuzu@isikun.edu.tr*
[d] *Istanbul Technical University, Mechanical Engineering Faculty, 34437, Istanbul, Turkey, bakkalmu@itu.edu.tr*

Abstract

This study examines the influence of cutting parameters on surface integrity, focusing on residual stress and surface roughness, in hot-forged and T6 heat-treated AA7075 components post-milling. Using the Taguchi L9 DOE method, orthogonal cutting milling experiments were performed, with residual stress measured via non-destructive X-ray diffraction (XRD). The analysis indicated that lower cutting speeds reduce residual stress, with down milling causing compressive and up milling causing tensile stresses. A proposed model showed a significant correlation between cutting force and residual stress—higher cutting forces increased residual stress. Surface roughness assessment revealed that feed rate greatly impacts residual stress, with lower feed rates reducing roughness. These insights will aid in developing a regression model for predicting outcomes in future experiments, enhancing the understanding and control of surface integrity in milling AA7075 components.

Keywords: Residual stress, Machining, Regression

1. Introduction

Surface integrity is crucial for defining a workpiece's operational capabilities, with residual stress being a significant influencing factor. Residual stresses affect properties such as fatigue life, corrosion resistance, and dimensional stability. Thus, comprehending machining and overall part quality necessitates an understanding of the residual stress induced during machining [1]. These stresses can be beneficial, like compressive residual stresses enhancing fatigue life and resistance to stress corrosion cracking, or detrimental, like tensile residual stresses reducing these properties and causing premature failure. Understanding residual stresses generated by machining processes is essential for optimizing machining parameters and improving part quality. Studies have highlighted the importance of optimizing cutting parameters to control residual stress profiles. Residual stresses induced by processes like turning and milling significantly influence the mechanical properties and performance of machined components, making their accurate prediction and control vital for high-performance applications. The presence of residual stresses can either enhance or detrimentally affect the functional behaviour of machined components. Depending on the process parameters used, the residual stresses left over from the machining process may be compressive or tensile [2]. Researchers have conducted extensive numerical analyses and experimental investigations to elucidate the correlation between residual stresses and cutting parameters in machining operations such as milling, turning, and hole drilling [3-4].

Yi et al. [5] investigated the influence of various milling parameters on residual stress in 7075-T7451 aluminum alloy. The study utilized orthogonal experiments to assess the effects of milling speed, feed per tooth, milling width, and cutting depth on the residual stress distribution. The most influential cutting parameter found was the feed per tooth (fz), which significantly affected the residual stress in both the feed direction and the vertical direction of feed during milling. Surface integrity studies on 7075 aluminium alloy after high-speed end milling, such as those conducted by Cai et al.[6], revealed that higher cutting speeds improve surface quality but also increase residual tensile stresses. Their work employed surface roughness measurements and X-ray diffraction to analyze the stress patterns, emphasizing the trade-off between surface finish and residual stress management.

With the advancement of technology, achieving quick results in fields such as automotive and aerospace industries, ideally at the lowest possible cost, provides significant advantages. For the numerical evaluation of residual stress, a challenging phenomenon to measure and predict, many methods have been developed, including destructive and non-destructive techniques.[7] A common aspect of both destructive and non-

destructive residual stress measurement methods is the necessity of specific sample preparation and setup times, which are generally high-cost processes. Due to the high production costs in industrial applications, non-destructive methods like XRD are more popular [8,9,10]. Therefore, predicting residual stress without the need for these methods is highly important. Finite Element Method (FEM) applications require substantial academic background and the licenses for FEM software are very expensive, making numerical calculations like regression the most suitable methods for industrial applications. Utilization of machine learning algorithms such as Support Vector Machines (SVM) in regression problems is one of the most popular numerical methods. Residual stresses induced by machining processes significantly impact the mechanical properties and performance of components. Support Vector Regression (SVR) has been extensively utilized for predicting these stresses, offering valuable insights for optimizing machining parameters. Hashemitaheri et al.[11] developed SVR models to predict maximum tool temperature and specific cutting force using a dataset of 196 samples, achieving high accuracy with mean squared error (MSE) values of 0.0015 and 0.0012 for training and testing data, respectively. Wang et al. [12] applied least squares support vector machines (LS-SVM) to predict surface roughness in the precision turning of lenses. They used chaotic particle swarm optimization and leave-one-out cross-validation on a dataset comprising turning parameters and 10 validation experiments. This method yielded an R^2 of 0.99887 and a mean absolute percent error (eM) of 8.96%. Additionally, Buyrukoğlu and Kesriklioğlu [13] employed SVR models to predict residual stresses in the turning of Inconel 718 and Ti6Al4V alloys, with sample sizes of 97 and 91, respectively. These models provided reliable predictions, highlighting the need for optimizing hyperparameters to achieve high accuracy. Collectively, these studies underscore the effectiveness and versatility of SVR in various machining and predictive applications, ensuring precise control over machining outcomes and enhancing overall process efficiency.

Previous studies in the literature have primarily focused on workpieces with simple geometric shapes that are not suitable for industrial conditions and do not include both hot forging and heat treatment. Additionally, predicting residual stress often involved conducting a large number of experiments to enable machine learning, which is not feasible in terms of cost and time for industrial conditions. Therefore, in this study, unlike the literature, a product from the automotive industry with a complex geometry, which has undergone hot forging and aging heat treatment, is used as the workpiece. Moreover, differing from the literature, the Taguchi L9 experimental design and Support Vector Regression method are employed to predict the residual stresses that may occur with different cutting parameters using a minimal number of experiments.

The main aim of this research is to examine how cutting parameters affect surface integrity, including residual stress and surface roughness, in hot-forged and T6 heat-treated AA7075 components after milling processes. The findings, such as cutting force, residual stress, and surface roughness, were utilized to develop a regression model for predicting future experiments. To understand the influence of cutting parameters, the non-destructive technique of X-ray diffraction was chosen to measure residual stress due to its efficacy in analyzing the impacts of cutting parameters on CNC milling experiments.

2. Materials and Methods

The material employed for the workpieces in this investigation was AA7075-T6, forged at the Birinci Otomotiv hot forging plant and its chemical and mechanical parameters are shown in Tables 1 and 2, respectively. Every sample was hot forged and T6 heat treated to provide similar cooling conditions, microstructure, and mechanical characteristics. The mechanical characteristics and chemical composition were determined by experiments.

Element	**Si**	**Fe**	**Cu**	**Mn**	**Zn**	**Cr**	**Ti**	**Al**
Content %	0.140	0.241	1.54	0.106	4.86	0.190	0.031	90.5

Table 1 Chemical compositions of the AA7075-T6 material

Ultimate Tensile Strength (MPa)	**Yield Strength (MPa)**	**Elongation (%)**	**Young Modulus (GPa)**	**Hardness (HBW)**	**Thermal conductivity, W/(m K)**	**Specific heat capacity, J/(kg K)**
540	476	11	71.7	170	130	0.960

Table 2 Physical and mechanical properties of the AA7075-T6 material

2.1 Experimental Methods

The machining experiments were conducted using vertical CNC machining center, specifically the Spinner VC-650 model, with a maximum spindle speed of 8000 rpm. The machining center, with a power rating of 16.5 kW, features an SK40 taper where a milling cutter was mounted. The experimental setup is illustrated in Figure 1. The work piece is secured to a fixture (as illustrated in Fig. 1 (b)) that is placed on top of a Kistler dynamometer (Type 9272) for measuring cutting forces. The selected face milling cutter for this study had a diameter (D) of 63 mm, with the specification İSCUR HM90 FAL-D063-27-16. The cutter was equipped with 3 evenly distributed carbide inserts, each having the specification HM90 APCR 160508R-P, only the face of the shaft was machined as shown in figure 3.

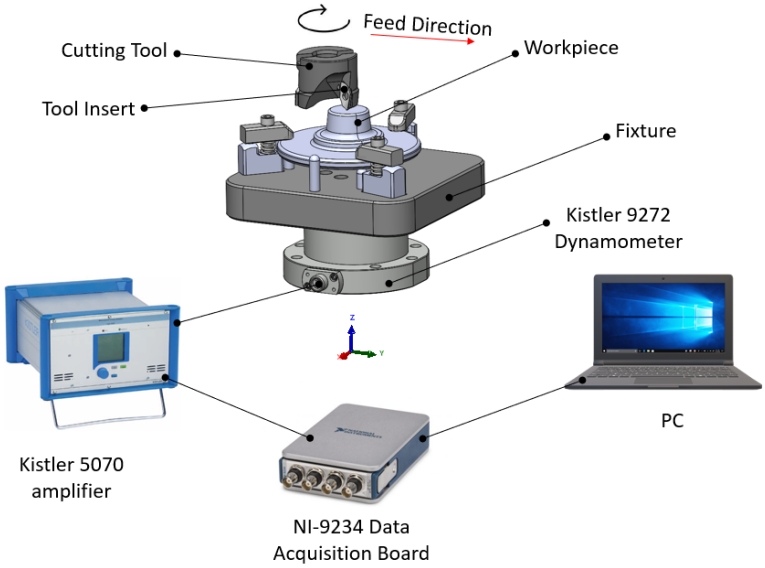

Figure 1: Schematic illustration of cutting force measurement experimental setup

A schematic representation of the center-face milling process is shown in Fig. 2. Here, f is the feed rate (mm/rev) and is calculated according to Eq 1, where f_t is the feed per tooth (mm/tooth) and z is the number of teeth of the tool, in our experiments the tool has 3 teeth (inserts) as mentioned before. n is the spindle speed and is used to calculate the cutting speed according to Eq 2.

$$f = f_t . z \quad (1)$$

$$V_c = \pi . D . n \quad (2)$$

The Taguchi method, employed as a design of experiments technique, aims to model, and analyse the influence of various parameters on the surface roughness and surface residual stresses of machined components. By utilizing orthogonal arrays design, this approach effectively reduces the number of experiments required by distributing variables in a balanced manner. Consequently, the necessary number of experiments is significantly decreased. In this study, the experiment was designed using the Taguchi L9 method, considering three factors: cutting speed, feed, and depth of cut, each investigated at three distinct levels, as shown in Table 3. It is known that in industrial applications, high feed rates and high depths of cut are used to reduce machining time, and the cutting parameters in this study closely align with those used by Birinci Otomotiv A.Ş, a company that carries out industrial applications in the automotive industry. All cutting tests in this research were

conducted under dry conditions. The milling of aluminium alloy workpieces took place in the environment depicted in Fig. 1. The milling process consisted of a single pass for each specimen, with a new insert used in each experiment. To observe the effect of milling direction, all experiments were conducted using up milling, except for experiment No. 1, which was performed using down milling.

Experiment #	Cutting Speed (m/min)	Feed per tooth (mm/tooth)	Depth of Cut (mm)
1	150	0.1	0.5
2	150	0.2	1
3	150	0.3	1.5
4	250	0.1	1
5	250	0.2	1.5
6	250	0.3	0.5
7	350	0.1	1.5
8	350	0.2	0.5
9	350	0.3	1

Table 3 Milling Parameter Set

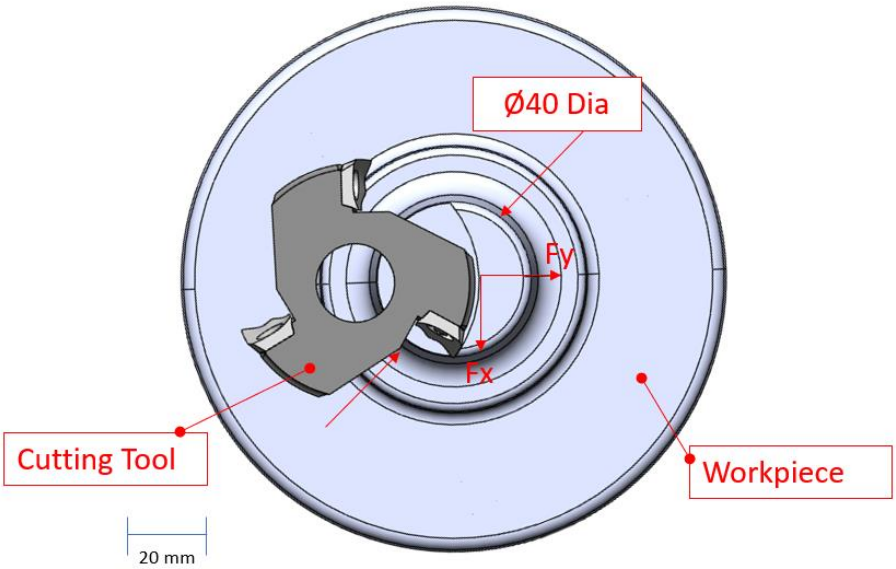

Figure 2: Schematic representation of the center-face milling

2.2 Residual Stress and Roughness Measurements

Residual stresses in the machined components were measured using the X-ray diffraction technique, a well-established non-destructive method that provides detailed information about the stress state within crystalline materials. XRD measures the spacing of crystal planes, which changes under the influence of residual stresses. The diffraction pattern obtained is used to calculate the strains and, subsequently, the stresses within the material. XRD is particularly suitable for measuring residual stresses because it can precisely determine the elastic strain by measuring the spacing between crystal planes (d-spacing) which is shown in fig 3. When a polycrystalline material undergoes elastic deformation, the strain is uniformly distributed over a substantial distance. This causes the lattice spacing within individual crystals to shift from its stress-free value to a new value, which is dictated by the applied stress. This process is explained by Bragg's law [6]
This measurement is based on Bragg's law which is defined in Eq. 3, which relates the angle at which X-rays are diffracted by the crystal planes to the distance between these planes. The basic principle involves directing X-rays at the material and measuring the angles and intensities of the diffracted beams. The changes in the diffraction angle provide information about the strains in the crystal lattice.

$$n\lambda = 2d\sin\theta \quad (3)$$

here, n signifies the diffraction order, λ refers to the wavelength of the X-rays, d denotes the distance between the planes in the crystal lattice, and θ is the angle at which diffraction occurs.

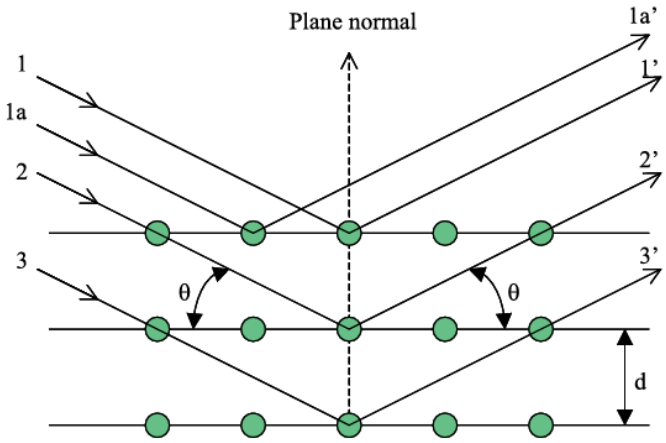

Figure 3: Diffraction of X Ray Beams by a Crystal Lattice.

The residual stress measurements were carried out using a diffractometer equipped with a Cu-Kα radiation source, which is commonly used for stress analysis due to its suitable wavelength for many engineering materials. The XRD equipment was calibrated using a stress-free reference sample to ensure accuracy. Measurements were taken at different teta (θ) angles to determine the variation in lattice spacing and calculate the stress tensor components [15,16] The fundamental equation used for determining macro residual stresses from diffraction measurements can be found by employing the principles of Hooke' s elasticity theory in references [14,10,17,18,19]

$$\varepsilon_{\phi\Psi} = \frac{1+\nu}{E}(\sigma_1\cos^2\phi + \sigma_2\sin^2\phi)\sin^2\Psi - \frac{-\nu}{E}(\sigma_1 + \sigma_2) \quad (4)$$

$$\sigma_\phi = \frac{E}{(1+\nu)\sin^2\Psi}\left(\frac{d_\Psi - d_n}{d_n}\right) \quad (5)$$

In this equation, $\varepsilon_{\phi\Psi}$ represents the strain at the ($\phi\Psi$) orientation, as defined in Figure 4. The term d_Ψ refers to the interplanar spacing measured in the stressed sample for the ($\phi\Psi$) orientation, while d_0 indicates the stress-free interplanar spacing. The stress tensor is denoted by σ_ϕ, and ν and E represent the Poisson's ratio and the Young's modulus of the material, respectively.

To construct the complete residual stress tensor in the plane of the newly created surface, measurements were obtained at three ϕ angles: 0°, 45°, and 90°. The normal stress (strain) for each ϕ angle was determined using the standard $\sin^2\Psi$ method. Then, the normal tensor coordinate transformation rules were utilized to compute the entire biaxial stress field ($\sigma_{\phi\theta}$, $\sigma_{\theta\theta}$, $\tau_{\phi\theta}$) on the newly formed workpiece surface within its coordinate framework. [20]

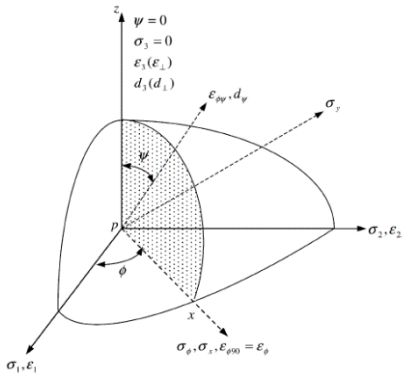

Figure 4: Schematic diagram of the principal stresses [16]

X-ray diffraction was utilized to evaluate the residual stress on the upper surface of the component depicted in Figure 5. The residual stress resulting from machining was measured using a Stresstech XStress 3000 G2R X-ray diffractometer, which employed radiation with a 3 mm diameter spot size. XRD measurements were conducted at a distance of 10 mm from the part's center. Residual Stresses in both Axial and Hoop direction was measured. After the stress measurement, Ra surface roughness values were measured using the Mitutoyo SJ 400 surface roughness measurement device, and the measurements are indicated in Table 5.

X-ray Diffraction Parameter	**Device Model**	**Radiation**	**Filter**	**2Θ**	**Miller Indices [h k l]**	**Penetration Depth (est.)**	**Collimator Size**
Specification/Values	XStress 3000 G2R	Cr - Kα	No Filter	156.7°	[2 2 2]	~ 20.0 µm	3 mm

Table 4 X-ray Diffraction Parameter

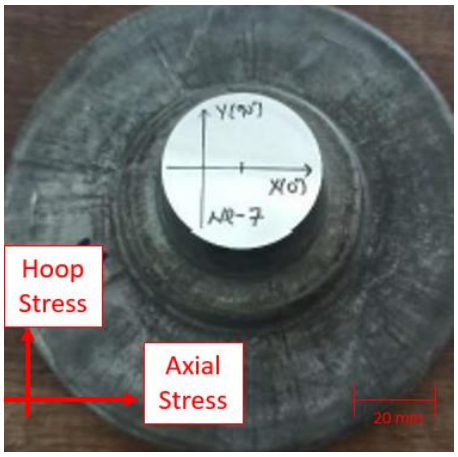

Figure 5: XRD Measurement sample for CNC milled for Exp. #7

2.3 Support Vector Regression Principle

Support Vector Regression (SVR) is a supervised learning algorithm derived from the Support Vector Machine (SVM) framework, initially developed for classification tasks. SVR extends the principles of SVM to regression problems, providing a robust method for function estimation in high-dimensional spaces. The fundamental idea behind SVR is to find a function that approximates the given data with a predefined accuracy, balancing model complexity and prediction accuracy.

The SVR algorithm operates by mapping the input data x into a higher-dimensional feature space $\varphi_{(x)}$ through a kernel function. This transformation enables the algorithm to handle complex,

nonlinear relationships between the input and output variables. In the feature space, a linear regression model is constructed, which can be expressed as:

$$y = \omega^T \varphi_{(x)} + b \tag{6}$$

where ω represents the weight vector, and b denotes bias term. SVR aims to determine the optimal ω and b that minimize the prediction error, ensuring that deviations from actual targets are within an acceptable margin ε. This objective is achieved by solving the following optimization problem:[20]

$$min\ (\omega, b, \xi, \xi^*) = \frac{1}{2}\omega^T\omega + C\left(\sum_{n=1}^{N}\xi_i + \sum_{n=1}^{N}\xi_i^*\right) \tag{7}$$

Subject to:

$$y_i - \omega^T\varphi(x_i) - b \leq \varepsilon + \xi_i \tag{8}$$

$$\omega^T\varphi(x_i) + b - y_i \leq \varepsilon + \xi_i^* \tag{9}$$

$$\xi_i, \xi_i^* \geq 0 \tag{10}$$

Here, ξ_i and ξ_i^* are slack variables allowing deviations beyond ε and C is a regularization parameter controlling the trade-off between model complexity and tolerance of deviations. Fig. 6 represent these notations and represent the transformation of kernel functions. Smaller values of $\|\omega\|$ contribute to the flatness of the estimated regression function, thereby reducing overfitting and complexity. The parameter C is crucial as it balances the trade-off between maintaining a flat regression function and allowing deviations within the margin ϵ\epsilonϵ. Proper selection of C is essential: a high value of C can lead to overfitting, while a low value may result in significant prediction errors.[21]

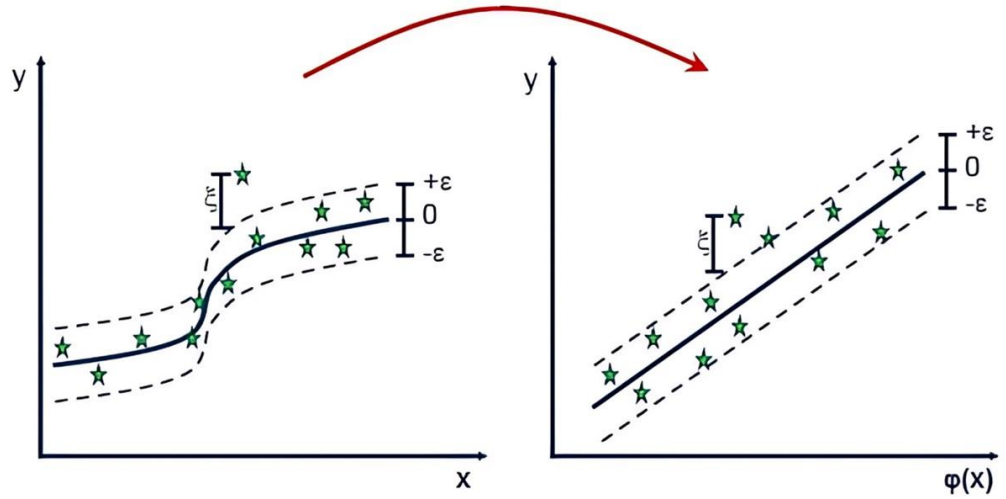

Figure 6: Kernell Function Transformation [23]

Additionally, the Karush–Kuhn–Tucker (KKT) conditions are employed to solve the nonlinear optimization problem and estimate the parameters ω and b. The solution to the regression problem is given by:

$$y = \sum_{i=1}^{N}(\alpha_i - \alpha_i^*)\, K\,(x_i, x)\ + b \tag{11}$$

where α and α^* are the Lagrange multipliers, and K (x_i, x) is the kernel function used to map the input data into the higher-dimensional space. Commonly used kernels include the radial basis function (RBF) and sigmoidal kernels. Selecting the appropriate kernel type and parameters, along with the values for C and ε, is critical for the performance of the SVR model.

In this research, SVR was used to predict residual stresses resulting from different machining parameters, such as spindle speed, feed rate, cutting depth, and tool type. Experimental data from controlled machining tests

were used to train the SVR model, with the RBF kernel chosen for its ability to capture nonlinear relationships in the data.

3. Result and Discussion

There are many factors influencing the residual stress of the milled surface, of which the most important ones are cutting speed (v), feed per tooth (f) , depth of cut (a_p) but, in the practical milling process, there are complicated nonlinear mapping relationships between these machining factors and the workpiece surface integrity such as residual stress and surface roughness, thus it's difficult to set regression model by mechanism analysis of milling process.

In this research, the experimental results obtained using the Taguchi L9 design are detailed in Table 5. A dynamometer was used to measure forces, and the moving average method was employed to compute the maximum force values in the X, Y, and Z directions. This method involved selecting 100 random points from the complete dataset to determine the maximum force values, which are summarized in Table 5. Also, in the table 5, the force measurements in the Y-axis, which is the feed direction, are observed to be higher compared to the force measurements in the X and Z axes. In the first three experiments with the lowest cutting speed of 150 m/min, it is observed that as the feed per tooth and depth of cut increase, the Fy max values significantly rise. Specifically, Fy max increases from 42.15 N to 742.8 N as the feed per tooth increases from 0.1 mm/tooth to 0.3 mm/tooth and the depth of cut increases from 0.5 mm to 1.5 mm. This indicates a strong correlation between the increase in both feed rate and depth of cut with the cutting force in the feed direction. The force in the feed direction (Fy max) shows a substantial increase from Experiment 1 to Experiment 3 due to higher feed rates and greater depths of cut.

Exp. No #	Cutting Speed (m/min)	Feed per tooth (mm/tooth)	Depth of Cut (mm)	$F_x max$ (N)	$F_y\ max$ (N)	F_z max (N)	R_a (µ)	Hoop Stress (MPa)	Axial Stress (MPa)
1	150	0.1	0.5	1.18	42.15	49.20	1.12	-108.7	-88.4
2	150	0.2	1	8.88	461.9	58.58	4.21	84	88.5
3	150	0.3	1.5	10.10	742.8	169.8	4.49	98.1	-58.8
4	250	0.1	1	5.460	256.5	44.40	2.44	93.1	64.9
5	250	0.2	1.5	7.022	428.1	78.61	2.3	73.4	49.7
6	250	0.3	0.5	4.305	207.2	51.65	3.95	81.8	-16.8
7	350	0.1	1.5	5.278	263.8	28.09	2.14	92.5	54.6
8	350	0.2	0.5	2.657	127.3	22.55	4.1	98.1	62.3
9	350	0.3	1	5.502	294.1	45.73	3.44	97.5	45.9

Table 5 Milling Parameter Set

Conversely, in the subsequent experiments with higher cutting speeds of 250 m/min and 350 m/min, a similar trend is noted. For instance, at a cutting speed of 250 m/min, F_{ymax} increases from 256.5 N to 428.1 N when the feed per tooth increases from 0.1 mm/tooth to 0.2 mm/tooth. The Cutting forces of the second three experiment rise as the feed rate and depth of cut increase. However, when examining the experiments at the highest cutting speed of 350 m/min, it is noticeable that while the feed rate increases, the measured F_{ymax} values also increase, but not as drastically as seen at lower speeds. For example, Fy max increases from 127.3 N to 294.1 N as the feed per tooth increases from 0.2 mm/tooth to 0.3 mm/tooth. increase in cutting forces of the last three experiment is less pronounced compared to lower speeds. This suggests that while feed rate is a significant parameter affecting cutting force, its impact is somewhat mitigated at higher cutting speeds.

Additionally, when the feed rate increases while the depth of cut decreases, such as in experiment 6 (cutting speed 250 m/min, feed per tooth 0.3 mm/tooth, depth of cut 0.5 mm), F_{ymax} is observed to be 207.2 N, which is lower compared to other setups with higher depths of cut. This indicates that depth of cut has a more pronounced effect on cutting force compared to feed rate. Furthermore, as the cutting speed increases, the observed change in force due to feed rate variations becomes less significant, highlighting the complex interplay between these cutting parameters.

In this study, various regression models were applied to predict surface integrity parameters. The models employed included Support Vector Regression (SVR), Ridge (L2 Regularization), and Lasso (L1 Regularization) regression models. The training and evaluation of these models were conducted using the Python programming language and the Scikit-Learn library. Each model was trained on 80% of the dataset and evaluated on a 20% test set. To assess the performance of the models, metrics such as Mean Squared Error (MSE), Mean Absolute Percentage Error (MAPE), and R-squared (R^2) were utilized.
Each model was further evaluated using the Leave-One-Out Cross Validation (LOO) method, which involves using each observation as test data while the remaining observations are used as training data. This approach allows for a more reliable assessment of the model's overall performance. At the end of the training process, the performance of each model on the test set was calculated, and the results were compared. Thus, in the milling operation mechanism, the relationship between cutting parameters, residual stress, and surface roughness was calculated with the help of a correlation matrix heat map, as seen in Figure 7.

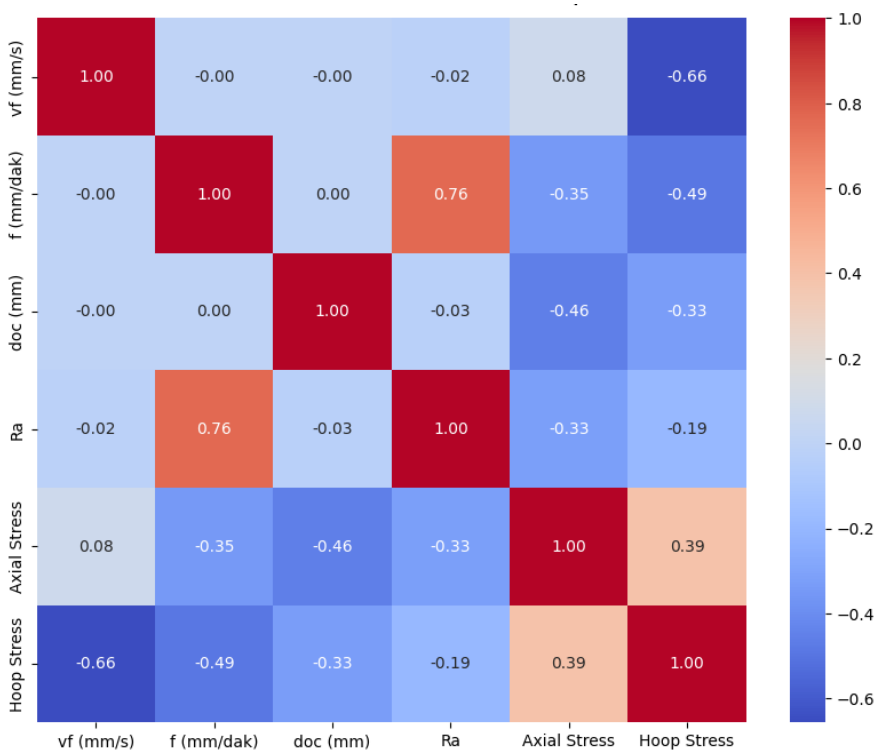

Figure 7: Correlation Matrix Heatmap for inputs and outputs of the regression analysis

3.1 Regression Analysis of the Cutting Parameters and Residual Stress

The impact of cutting parameters on residual stress was evaluated using Lasso, Ridge, and Support Vector Regression (SVR) models. The residual stresses measured were axial residual stress and hoop stress. Table 6 summarizes the performance metrics of the regression models. Lasso regression resulted in a mean squared error (MSE) of 0.15 for axial residual stress and 0.07 for hoop stress, with mean absolute percentage error (MAPE) values of 13.1% and 15.5%, respectively. Ridge regression performed similarly, with an MSE of 0.15 for axial residual stress and 0.06 for hoop stress, and MAPE values of 13.0% and 14.5%. The SVR model outperformed both Lasso and Ridge, achieving an MSE of 0.12 for axial residual stress and 0.06 for hoop stress, with MAPE values of 11.5% and 15.0%

Model	**MSE (Axial Residual Stress)**	**MSE (Hoop Stress)**	**MAPE (Axial Residual Stress)**	**MAPE (Hoop Stress)**
Lasso Regression	0.15	0.07	13.1%	15.5%
Ridge Regression	0.15	0.06	13.0%	14.5%
SVR	0.12	0.06	11.5%	15.0%

Table 6: Performance of Regression Models on Residual Stress

The regression analysis highlighted the significant impact of cutting parameters on residual stresses. Higher cutting speeds generally resulted in lower residual stresses due to the thermal softening effect. Increased feed rates led to higher residual stresses, likely due to the greater mechanical load imposed on the material. Depth of cut was also a critical factor, with deeper cuts inducing higher residual stresses due to the increased material removal rate. As it seen in the figure 7, For the Hoop Stress, the most influential parameters are cutting speed, feed per tooth, and depth of cut respectively, for the axial stress the most influential parameters are depth of cut, feed per tooth and cutting speed respectively.

3.2 Regression Analysis of the Cutting Parameters and Surface Roughness

Surface roughness (Ra) was also predicted using Lasso, Ridge, and SVR models. The analysis showed that the cutting parameters significantly influenced the surface roughness of the machined components. Table 7 presents the performance metrics of the regression models for surface roughness prediction. Lasso regression achieved an MSE of 0.18 and a MAPE of 12.7%. Ridge regression had an MSE of 0.17 and a MAPE of 12.2%. SVR again provided the best performance, with an MSE of 0.14 and a MAPE of 11.0%.

Model	MSE (**Ra**)	MAPE (**Ra**)
Lasso Regression	0.18	12.7%
Ridge Regression	0.17	12.2%
SVR	0.14	11.0%

Table 7: Performance of Regression Models on Surface Roughness

The regression analysis revealed that higher cutting speeds tended to improve surface finish, resulting in lower Ra values. Conversely, higher feed rates and deeper cuts generally resulted in increased surface roughness due to the higher mechanical load and increased cutting forces. As it is seen in the figure 7, the most influential parameters are feed per tooth, depth of cut and cutting speed respectively.

3.3 Comparison of the Regression Methods

Comparing the three regression methods, SVR consistently outperformed both Lasso and Ridge in predicting both residual stresses and surface roughness. The superior performance of SVR can be attributed to its ability to capture the nonlinear relationships between the cutting parameters and the output variables through the use of the radial basis function (RBF) kernel.

Metric	**Lasso**	**Ridge**	**SVR**
MSE (Axial Stress)	0.15	0.15	0.12
MSE (Hoop Stress)	0.07	0.06	0.06
MAPE (Axial Stress)	13.1%	13.0%	11.5%
MAPE (Hoop Stress)	15.5%	14.5%	15.0%
MSE (Ra)	0.18	0.17	0.14
MAPE (Ra)	12.7%	12.2%	11.0%

Table 8: Comparative Performance of Regression Models

The practical implications of these findings suggest that SVR is the most suitable one among the three algorithms utilized for predicting machining outcomes in terms of residual stresses and surface roughness. This model's ability to accurately predict these parameters can help optimize the cutting process, leading to better surface integrity and performance of machined components.

4. Conclusions

In this comprehensive study, the effects of milling parameters on the surface integrity of hot-forged and T6 heat-treated AA7075 components were systematically examined. Utilizing the Taguchi L9 experimental design, the investigation provided significant insights into the relationship between cutting parameters, residual stress, and surface roughness.

- The study indicated that force measurements in the Y-axis (feed direction) were higher compared to the X and Z axes. For instance, in the first experiment, the Fy max value was 42.15 N, whereas Fx max and Fz max were 1.18 N and 49.20 N, respectively. As the feed rate and depth of cut increased, the forces also escalated, with Fy max reaching up to 742.8 N in the third experiment.
- The findings revealed that cutting speed and feed rate are crucial factors influencing residual stress. Lower cutting speeds (150 m/min) and down milling conditions were found to reduce residual stress significantly. Down milling induced compressive residual stress, with values reaching as low as -108.7 MPa, while up milling resulted in tensile stress, with values up to 98.1 MPa. The relationship between cutting parameters and residual stress can vary across different studies in the literature. Findings such as the reduction of residual stress with decreasing cutting speed are supported by the work of Mehmet E. Kara et al. on CGI material [14] and the study conducted by Yue, Qibin, et al. on 7075-T6 material [24]. The SVR, Lasso, and Ridge regression models were employed to predict these stress variations, with SVR showing the highest accuracy, achieving an MSE of 0.12 for axial residual stress and 0.06 for hoop stress.
- The analysis demonstrated that feed rate had the most substantial impact on surface roughness. Higher feed rates (0.3 mm/tooth) led to increased roughness, with Ra values ranging from 1.12 µm to 4.49 µm. The regression models confirmed these observations, with SVR outperforming Lasso and Ridge. SVR achieved an MSE of 0.14 and a MAPE of 11.0% in predicting surface roughness.
- By integrating experimental data and advanced regression techniques, a robust predictive model was developed. This model successfully correlated cutting parameters with residual stress and surface roughness, offering a valuable tool for optimizing milling operations. The correlation matrix heatmap illustrated in Figure 7 further validated these relationships, showing a strong correlation between cutting parameters and both residual stress and surface roughness.
- The regression analysis using Lasso, Ridge, and SVR demonstrated that SVR is the most effective model among the three algorithms utilized for predicting residual stresses and surface roughness based on cutting parameters. The insights gained from this analysis can inform the optimization of milling processes, enhancing the quality and performance of machined AA7075 component.

The practical implications of these findings are significant, providing a pathway to optimize milling parameters to enhance the surface integrity and performance of AA7075 components. By leveraging the predictive capabilities of the SVR model, manufacturers can achieve better control over machining outcomes, leading to improved component quality and operational efficiency.
Future research could expand on this work by exploring other alloy systems and incorporating real-time monitoring technologies to further refine predictive models and machining practices.

Acknowledgements
The authors would like to thank the Birinci Otomotiv A.Ş for the financial and equipment support and Simultura Material Technologies Inc. for residual stress measurements.

References

[1] Reimer, A., and X. Luo. "Prediction of Residual Stress in Precision Milling of AISI H13 Steel." *Procedia CIRP*, vol. 71, 2018, pp. 329-334. doi:10.1016/j.procir.2018.05.036.
[2] Liang, S. Y., and J.-C. Su. "Residual Stress Modeling in Orthogonal Machining." *Annals of the CIRP*, vol. 56, no. 1, 2007, pp. 65-68. doi:10.1016/j.cirp.2007.05.018.
[3] Berry, Luke, et al. "The Influence of Milling Induced Residual Stress on Fatigue Life of Aluminum Alloys." *Forces in Mechanics*, vol. 7, 2022, p. 100096. doi:10.1016/j.finmec.2022.100096.
[4] Capello, Edoardo. "Residual Stresses in Turning Part II: Influence of the Machined Material." *Journal of Materials Processing Technology*, vol. 172, no. 2, 2006, pp. 319-326. doi:10.1016/j.jmatprotec.2005.10.009.
[5] Yi, Shouhua, et al. "Experimental Analysis and Prediction Model of Milling-Induced Residual Stress of Aeronautical Aluminum Alloys." *Applied Sciences, vol. 11, no. 13, 2021, p. 5881. doi:10.3390/app11135881.*
[6] Cai, X. J., Ming, W. W., and M. Chen. "Surface Integrity Analysis on High Speed End Milling of 7075 Aluminum Alloy." Advanced Materials Research, vol. 426, 2012, pp. 321-324. doi:10.4028/www.scientific.net/AMR.426.321.
[7] Cheng, Minghui, et al. "Prediction of Surface Residual Stress in End Milling with Gaussian Process Regression." Measurement, vol. 178, 2021, p. 109333. doi:10.1016/j.measurement.2021.109333.
[8] Díaz, Felipe, Claudio Mammana, and Armando Guidobono. "Evaluation of Residual Stresses Induced by High Speed Milling Using an Indentation Method." Modern Mechanical Engineering, vol. 2, 2012, pp. 143-150. doi:10.4236/mme.2012.24019.
[9] Soori, Mohsen, and Behrooz Arezoo. "A Review in Machining-Induced Residual Stress." Journal of New Technology and Materials, vol. 12, no. 1, 2022, pp. 64-83. doi:10.1016/j.jntm.2022.109333.
[10] Luo, Quanshun. "A Modified X-ray Diffraction Method to Measure Residual Normal and Shear Stresses of Machined Surfaces." The International Journal of Advanced Manufacturing Technology, vol. 119, 2022, pp. 3595-3606. doi:10.1007/s00170-021-08645-4.
[11] Hashemitaheri, Maryam, et al. "Prediction of Specific Cutting Forces and Maximum Tool Temperatures in Orthogonal Machining by Support Vector and Gaussian Process Regression Methods." *Procedia Manufacturing*, vol. 48, 2020, pp. 1000-1008. doi:10.1016/j.promfg.2020.05.139.
[12] Wang, Xingsheng, et al. "Predictive Modeling of Surface Roughness in Lenses Precision Turning Using Regression and Support Vector Machines." *The International Journal of Advanced Manufacturing Technology*, vol. 87, 2016, pp. 1273-1281. doi:10.1007/s00170-013-5231-3.
[13] Buyrukoğlu, Selim, and Sinan Kesriklioğlu. "A Comparison of Ensemble and Base Learner Algorithms for the Prediction of Machining Induced Residual Stresses in the Turning of Aerospace Materials." *Bitlis Eren University Journal of Science*, vol. 11, no. 3, 2022, pp. 861-879. doi:10.17798/bitlisfen.1130044.
[14] Kara, Mehmet Emre, Ali Taner Kuzu, and Mustafa Bakkal. "Investigation of Residual Stresses Induced by Milling of Compacted Graphite Iron by X-ray Diffraction Technique." *Journal of Materials Engineering and Performance*, 2023. doi:10.1007/s11665-023-08904-3.
[15] Huang, Xiaoming, et al. "An Experimental Investigation of Residual Stresses in High-Speed End Milling 7050-T7451 Aluminum Alloy." *Advances in Mechanical Engineering*, vol. 2013, Article ID 592659, 7 pages. doi:10.1155/2013/592659.
[16] Prevéy, Paul S. "Current Applications of X-ray Diffraction Residual Stress Measurement." *Developments in Materials Characterization Technologies*, edited by G. Vander Voort and J. Friel, ASM International, 1996, pp. 103-110.
[17] Masoudi, Soroush, et al. "Effect of Machining-Induced Residual Stress on the Distortion of Thin-Walled Parts." *The International Journal of Advanced Manufacturing Technology*, vol. 76, 2015, pp. 597-608. doi:10.1007/s00170-014-6281-x.
[18] Berry, Luke, et al. "The Influence of Milling Induced Residual Stress on Fatigue Life of Aluminum Alloys." *Forces in Mechanics*, vol. 7, 2022, p. 100096. doi:10.1016/j.finmec.2022.100096.
[19] Wu, Qiong, Da-Peng Li, and Yi-Du Zhang. "Detecting Milling Deformation in 7075 Aluminum Alloy Aeronautical Monolithic Components Using the Quasi-Symmetric Machining Method." *Metals*, vol. 6, no. 80, 2016, pp. 1-14. doi:10.3390/met6040080.
[20] Huang, Xiaoming, Jie Sun, and Jianfeng Li. "Effect of Initial Residual Stress and Machining-Induced Residual Stress on the Deformation of Aluminium Alloy Plate." *Journal of Mechanical Engineering*, vol. 61, no. 2, 2015, pp. 131-137. doi:10.5545/sv-jme.2014.1897.

[21] Yeganefar, Ali, Seyed Ali Niknam, and Reza Asadi. "The Use of Support Vector Machine, Neural Network, and Regression Analysis to Predict and Optimize Surface Roughness and Cutting Forces in Milling." *The International Journal of Advanced Manufacturing Technology*, vol. 105, 2019, pp. 951-965. doi:10.1007/s00170-019-04227-7.
[22] Wu, Deh. "Surface Hardness Intelligent Prediction in Milling Using Support Vector Regression." *Fourth International Conference on Natural Computation*, IEEE, 2008, doi:10.1109/ICNC.2008.258.
[23] Sayad, Saed. "Support Vector Machine Regression." *Saed Sayad's Homepage*. Accessed July 11, 2024. https://www.saedsayad.com/support_vector_machine_reg.htm.
[24] Yue, Qibin, et al. "Modeling and Optimization of Surface Residual Stress Profiles in Milling of Aluminum 7075-T6 Alloy." *The International Journal of Advanced Manufacturing Technology*, vol. 130, no. 1, 2024, pp. 5913-5934. Springer-Verlag London Ltd